COMPUTATIONS OF POROSITY AND PERMEABILITY OF SPARIC CARBONATE USING MULTI-SCALE CT IMAGES

Abraham S, Grader, Ingrain Inc., Andrew B.S. Clark, Abu Dhabi Company for Onshore Oil Operations (ADCO), Taha Al-Dayyani, Abu Dhabi Company for Onshore Oil Operations (ADCO), and Amos Nur, Ingrain Inc.,

This paper was prepared for presentation at the International Symposium of the Society of Core Analysts held in Noordwijk, The Netherlands 27-30 September, 2009

ABSTRACT

The determination of fluid flow properties in carbonate rocks is strongly affected by heterogeneity. This paper presents a case study that describes the heterogeneity of a carbonate sample. Then, through multi-scale x-ray CT imaging, core panoscopy, a base flow unit in the sample was selected for property computation. Volumes scanned at different resolutions and fields of view that are spatially registered are presented. Using digital rock physics the proper transport properties of the core were determined. The flow unit is a bio-sparic portion of the sample that fills the spaces between large solid carbonate fragments. High-resolution micro-CT imaging provided a digital sample which was the basis for calculating porosity, permeability, and relative permeability for the sample using the Lattice Boltzmann fluid dynamics method. The resulting digital rock physics computations were in good agreement with the laboratory measurements that were released and made available for this publication.

INTRODUCTION

Reservoir rock material collected during drilling is one of the main sources used to derive reservoir fluid transport and rock mechanics properties. Carbonate reservoirs may have heterogeneities that create multi porosity/permeability systems that are very difficult to describe and to determine their flow properties. They may contain micritic, sparic, and much larger grain and pore structures, all in one reservoir and in close proximity. For Example, in the Arab formations in Saudi Arabia *Cantrell and Hagerty* (1999) developed four categories for micro-porosity. Conventional methods use laboratory procedures to perform experiments that yield directly or indirectly required rock properties. Some of the procedures, such as the determination of relative permeabilities, may take several months to perform. Also, in some cases, it is very difficult, or impractical to perform the experiments in the first place. Yet, as reservoir characterization is becoming ever more important for oil and gas production, a much larger portion of reservoir rocks than what are currently evaluated, from cuttings to full cores, will need to be analyzed. Digital rock physics stem from the availability of high-resolution x-ray CT images. Various rock properties can be determined from digital rock volumes such as acoustic properties (Knackstedt et el. (2009), Dvorkin and Nur (2008), Dvorkin et al. (2009)), elastic properties (Knackstedt et al. (2002), Youngseuk et

al. (2002)), and fluid flow properties (Touati et al. (2009), Alvarado et al. (2006), Knackstedt et al. (2004)).

This paper offers an example of the use of digital rock physics do determine porosity, permeability, and relative permeabilities for a carbonate sample using multi-scale imaging. Digital rock physics using the Lattice Boltzmann Method (LBM) for fluid dynamic calculations is at a point where it can calculate reasonably correct flow properties given a proper digital representation of the pore space (Boltzmann, (1896), Chapman, (1970), Bhatnagar (1954), Gunstensen (1991), Shan and Chen (1993), Swift et al. (1995), D'Humieres et al. (2002)). The main issue facing digital rock physics is the need to up-scale the computed properties to the scale of the core. Further up scaling processes to the field scale are done using geo-statistical models and are not the subject of this paper.

The process presented in this paper includes sample preparation, imaging, image processing, property computations, and property integration to the core scale. Multi-scale imaging has become an integral part of scientific research in the material science, including resolutions in the nano-meter scales (Principe, (2002), Principe, (2007), Tkachuk, et al. (2007)). The sample is subjected to a descending scale of x-ray CT imaging, along with physical sub-sampling. The descending size of scanning leads to increased resolution of the three-dimensional digital core. The low-resolution/large-field-of-view images guide decisions about the location and size of higher-resolution/smaller-field-of-view scans and physical sub-samples. This process allows consistent registration of samples and images of different size and resolution, i.e. we know where the high-resolution volume is located inside the low-resolution one. The resulting digital images are segmented and the pore structure is determined on the x-ray CT grid system. The resulting three-dimensional pore structure, that is the same as the actual pore structure subject to resolution limits, is used as the input grid system for direct fluid dynamic computations. These computations represent the Navier-Stokes fluid flow equations to the second order of accuracy. They yield absolute permeability, relative permeabilities, and capillary pressure. The porosity is determined directly from the segmented images. In this paper we focus only on porosity and permeabilities. Multiple scale imaging permits the estimation of properties at the core scale. The intension of this paper is to demonstrate the use of the method for one carbonate example.

THE SAMPLE

The lithofacies from which the plug was cut is a coated grain, skeletal, rudstone-floatstone limestone. The larger skeletal fragments consist of Rudist fossils. The original conventional core was cut from vertical oil producing well, at approximately 8000 ft subsea. The age of the reservoir is Barremian-Aptian (Lower Cretaceous). The carbonate plug (25 mm in diameter and about 50 mm in length) was taken from a continuous core (Figure 1a). A disk from one end of the plug was used for thin section work. The rest of the sample was then used to measure permeability and relative permeability in a physical lab. Then, the sample was cut and a portion of it (about 12 mm in length) was send to Ingrain for digital rock physics (Figure 1b), and another portion of the sample was used for MICP work. The main purpose of the work presented in this paper was to estimate the flow properties of the portion of the

carbonate that is made up of small calcite crystals and skeletal remains on the order of 100 micron range, and to relate this information to larger scales of the core.

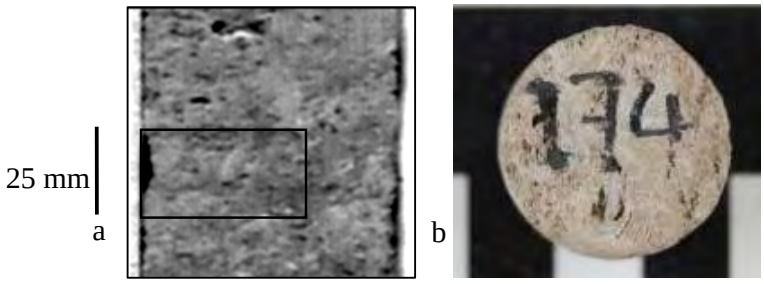

Figure 1: a: Photograph of the large core in its barrel, plug region highlighted. b: Photograph of the plug face that was used for digital rock physics. Plug diameter is 25 mm.

MULTI-SCALE IMAGING PROCESS

The sample used for digital rock physics was about 25% in length of the sample that was used for fluid flow lab measurements (12 mm out of 50 mm). The cylindrical sample was placed in the x-ray field and the entire sample was used to create a shadowgraph (radiograph) – a single view of the sample that is described later. Then two regions of the sample were scanned without cutting the sample. Each scan had diameter had height of 8 mm, covering about 9% of the total volume of the sample. After the sample was cut, two types of scans were acquired. The first type was a medium- resolution with a field of view of 4 mm, covering about 1% of the volume of the original sample. The second type was a high-resolution micro-CT scan with a field of view of 2 mm, amounting to about 0.1% of the original volume.

A low-resolution (8 micron pixels) two-dimensional projection of the sample was acquired in order to decide what part of the core should be selected for micro-CT. If this sample were the entire plug on which physical measurements were made, the entire sample would have been scanned to provide the ability to define flow units. Since this was only about one fifth of the original plug, the above step was simplified. Figure 2a shows the two-dimensional projection of the sample. This is a reverse gray scale color scheme in which the dark areas represent higher density and the light gray areas represent low density (the reverse of the way CT data are typically presented). It shows two distinct regions: a low density rather homogeneous region (solid circle), and a high density heterogeneous region (dashed circle). The circles indicate 8 mm diameter regions that were selected for micro-CT as the first stage in generating the three-dimensional digital cores. Examples of two-dimensional slices of the CT images are shown adjacent to the projection.

The vuggy region with higher density to the right (Figure 2b) shows three main structures: large dense shell fragments, large pores that are isolated from each other (to be discussed later in the paper), and high porosity regions with grains and fragments on the order of 100 microns, that will be shown later to control the flow properties of the sample. The more porous region is shown on the left (Figure 2c). In this slice about half the space is occupied by a solid grain, and the other half is the high porosity substance that is filling some of the inter-shell volumes in the vuggy region to the right.

These two low-resolution scans were performed in sub-volume mode, in which the sample is mounted eccentrically and 8 mm diameter volumes are imaged out of a 25 mm diameter core. To scan at higher resolution, in order to maximize signal-to-noise ratios, the core must be physically sub-sampled.. A 0.125 mm diameter wire saw was used to divide the sample into small pillars that could then be scanned at higher resolution than the original images (Figure 3a). The low resolution three-dimensional CT images guided the physical sub-sampling of the core.

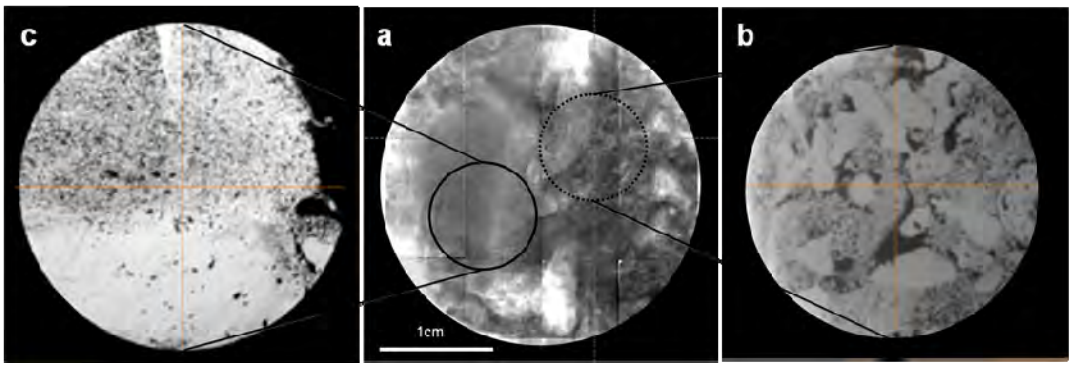

Figure 2: a: Two-dimensional projection of the sample. b: Low-resolution single CT slice out of the three-dimensional volume of a high density vuggy region. c: Low-resolution CT single slice of a low density porous region. CT voxel size is 8 microns.

A pillar sized 8-by-8 mm was cut from vuggy region. (see Figure 2b). It was scanned at a partial diameter ratio of about 0.5, resulting in 4 micron voxels. A slice of this CT image is shown in Figure 3b.

The pillar cut from the highly porous region is 4 mm on the side. It was positioned in the scanner so that a large porous region would be captured in the image, based on the low-resolution scan. The single slice shown in Figure 3c is almost completely in the desired region, with little of the large solid grain or shell material, visible in low-resolution image (Figure 2c). The image reveals a mixture of small grains and shell fragments on the order of 100 microns in size.

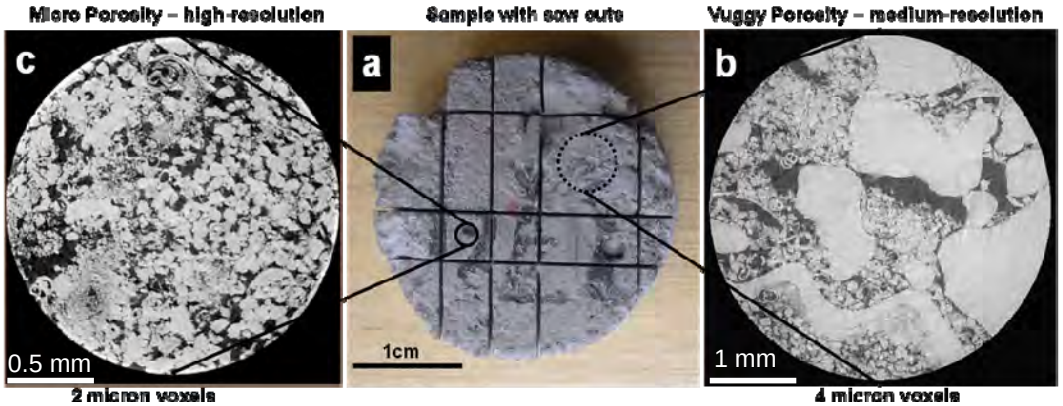

Figure 3: a: A photograph of the sample after it was cut into smaller rectangular pillars. b: A medium-resolution CT single slice of the vuggy region of the sample showing shell fragments (white), large pores (large black patches) and the porous matrix portion of the space filled with calcite fragments and crystals. c: A high-resolution single CT slice showing the material of interest, the porous matrix of the sample.

Thus we scanned each region of interest twice. The vuggy region was scanned with 8 microns (low resolution) and 4 micron (medium resolution) voxels. The two volumes are registered (Figure 4a), though they are not concentric. The low-resolution volume was used to select a typical volume suited for medium-resolution scanning. The medium-resolution scan (Figure 4b) was used in the porosity and permeability calculations while the low-resolution scan was used to determine the fractions of a) the large vuggy porosity, b) the porous granular material and c) the solid high density shell fragments.

The portion of the rock that includes large volumes of the granular filling calcite has been scanned at a high-resolution, 2 micron voxels, and is registered to the low-resolution scan, internally (Figure 5a). It is also shown separately on the right (Figure 5b). The low-resolution scan identified clearly where the next resolution scan should take place so that the resulting image will maximize the fraction of the granular filling porosity.

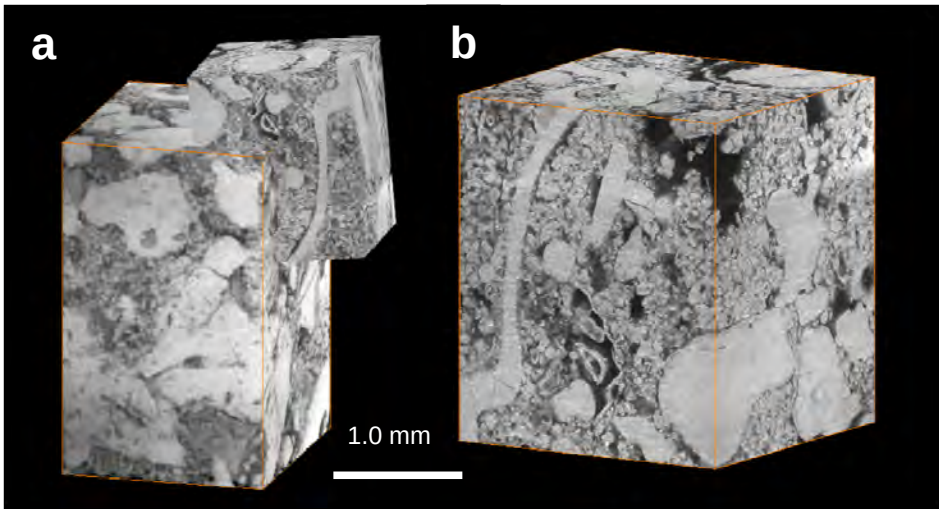

Figure 4: a: Two three-dimensional images of different resolutions registered in the same spatial domain. The low-resolution one has voxels of 8 microns. The medium-resolution image has 4 micron resolution. b: A medium-resolution volume of the vuggy region of the core.

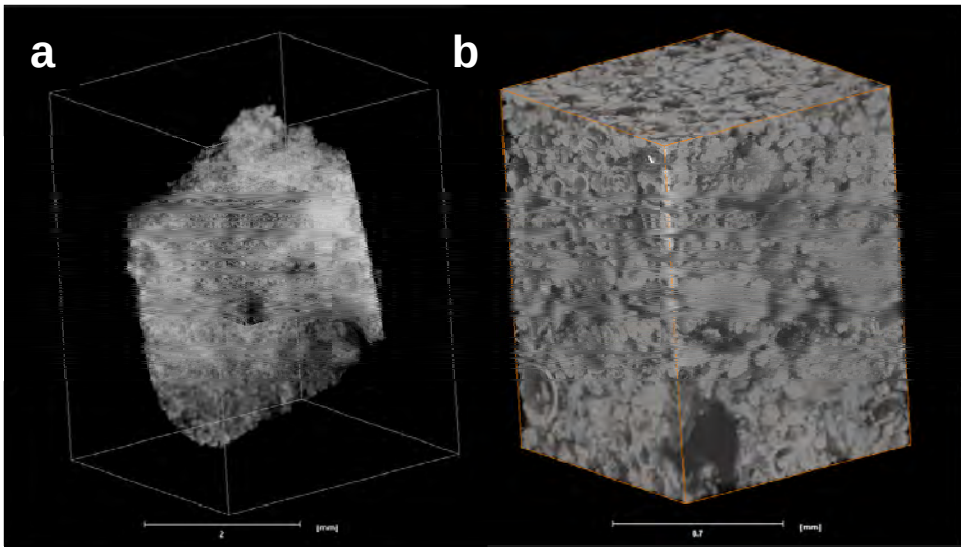

Figure 5: Granular porosity: a: Two three-dimensional volumes of different resolutions registered in the same spatial domain. The low-resolution one has voxels of 8 microns. The high-resolution image has 2 micron resolution. b: A high-resolution volume of the granular porosity region of the core.

ANALYSIS: POROSITY

The digital sample shown in Figure 5b (high-resolution with 2 micron voxels) was used to compute porosity for the granular portion of the sample at 0.29. The low resolution granular region that was scanned exhibits a transition from granular material to about 50% large solid grains, shown in Figure 6. The distance between each slice is 0.85 mm. The first slice (stack position 300/1000), Figure 6a, shows that about half the area is granular and the other half is solid. Two micro fractures can be seen in the lower left of the slice. The second slice (stack position 400/1000), Figure 6b, shows an increase in the fraction of the granular material. The last slice on the right (stack position 700/1000) shows the entire area occupied by granular material along with a worm hole shown as the large dark region. In this low resolution scan about 70% of the volume is granular leading to an overall porosity of about 0.21.

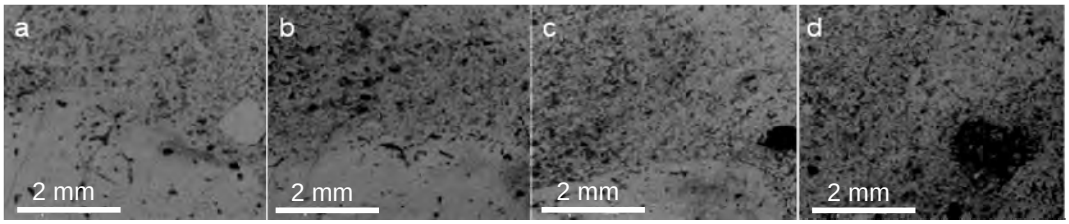

Figure 6: Four slices of the granular region, low-resolution, 8 micron voxels. These images are about 0.85 mm apart and show a transition to the granular material, from left to right.

The digital sample with the large shell fragments shown in Figure 4a (low resolution micro-CT with 8 micron voxels) was used to compute three fractions: the dense shell fragments with negligible porosity with a bulk volume fraction of 0.500; the large pores system with a bulk volume fraction of 0.065, and the bulk volume fraction of the porous granular system at 0.435. The large pore system, when segmented on its own, is

disconnected. The connection to the flowing portion of the porosity is through the porous granular fraction. The disconnected large pore structure is shown in Figure 7. Based on a granular porosity of 0.29, and a fraction of the granular material of 0.435, the total porosity of the region with the large shell fragments is about 0.19.

The entire core plug was not scanned before it was divided into three parts. Therefore, the entire heterogeneity of the sample was not captured by imaging. The two-dimensional projection (Figure 2a) shows that, at least for the portion of the sample that was considered, about half of the sample can be characterized by a mixture of granular material and the other half by the region that contains large shell fragments. Thus, the average porosity of the sample used in this study is about 0.20. The MICP data on another portion of the sample provided a porosity value of 0.21. The porosity of the entire sample prior to dividing it into three parts was 0.25, as determined by an external laboratory. The variability of porosity in different regions of the sample leads to the differences in the porosity estimates shown here. The CT-derived porosity usually underestimates the physical porosity due to the limit posed by resolution.

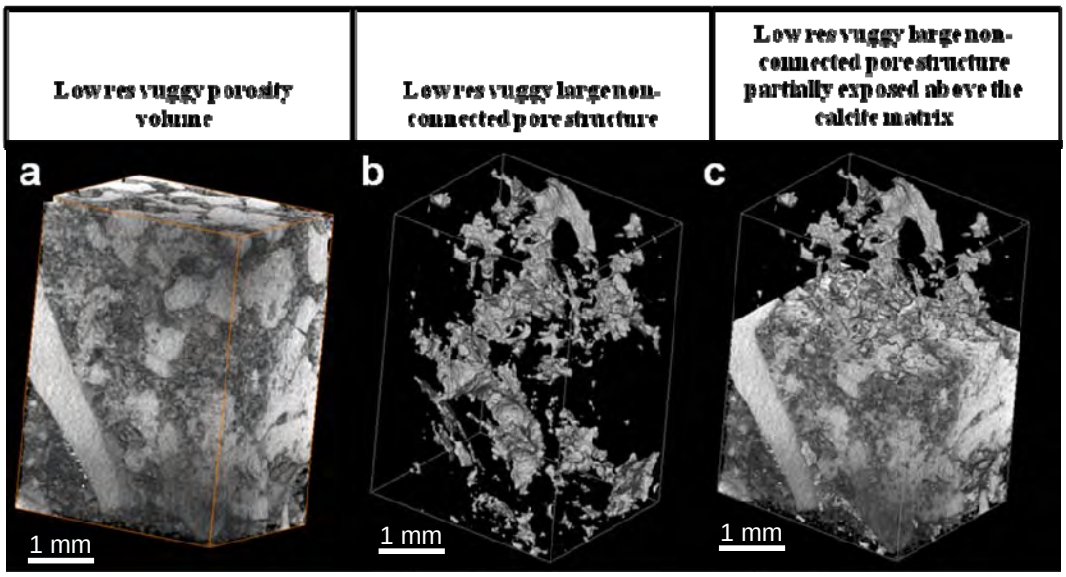

Figure 7: Low-resolution vuggy volume showing the disconnected large pores.

ANALYSIS: PERMEABILITY

The absolute permeabilities of the two regions were computed using the Lattice Boltzmann Method (LBM) in single-phase mode. The first region was for the granular volume shown in Figure 5b, yielding 1.19 D (matrix size 350x350x350). The second region was the vuggy volume shown in Figure 4b, yielding 1.2 D (matrix size 652x641x751). The total core permeability measured by and external lab was 0.44 D. Considering that the lab measurement represents about three times the volume and the overall heterogeneity of the sample, the CT-derived permeability is reasonable. Moreover, as the entire sample was not scanned, no attempt was made to integrate the two CT permeabilities. The permeability of the granular material controls the system.

In the vuggy regions, fluid must flow through the granular regions, as the large pore structure is not connected. It is a flow in series, and the presence of the large pore structure increases the permeability in proportion to its length fraction, if it were equally distributed in space. If the large pore structure was directly connected, the permeability of the sample would be much larger than the permeability of the granular fraction.

The granular volume shown in Figure 5b was used to compute relative permeabilities using LBM in two-phase mode. Reservoir fluid properties and reservoir wetting characteristics were used directly on the CT-derived pore structure. These include a viscosity ratio of 2/3 and an interfacial tension of 1 dyne/cm. The relative permeabilities and permeability ratio are shown in Figures 8a and 8b, respectively.
The material presented in this paper is part of a large study and exact details of the matches between the relative permeabilities shown here and ones physically measured in the laboratory cannot be published at this time. Relative permeability results, initial water saturation and residual oil saturation that were calculated through imaging were compared with the available simulation model data for the same rock type. The initial water saturation and residual oil saturation were calculated through CT/LBM to be 5% and 80% respectively , compared with 4% and 85% from simulation model. A good agreement between Kro from the study and SCAL data used for simulation model is indicated. However, Krw from the CT-calculated data and the SCAL results are in reasonable match only up to water saturation of 50%. A detailed comparison will be carried out when a wide range of samples from the same environment will be analyzed.

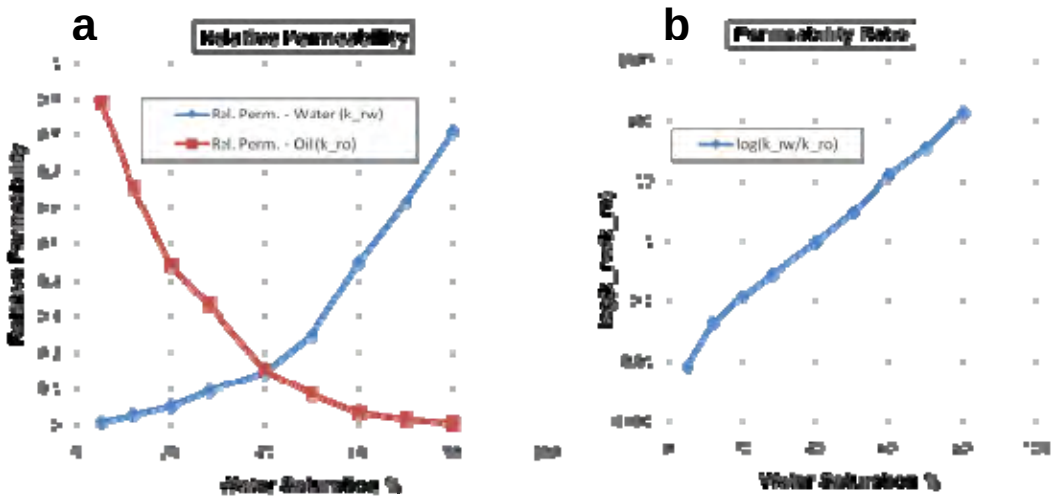

Figure 8: Relative permeabilities (a) and permeability ratio (b) as a function of water saturation for the granular portion of the sample (matrix size 350x350x350).

The material presented in this paper is part of a large study and exact details of the matches between the relative permeabilities shown here and ones physically measured in the laboratory cannot be published at this time. Relative permeability results, initial water saturation and residual oil saturation that were calculated through imaging were compared with the available simulation model data for the same rock type. The initial water saturation and residual oil saturation were calculated through CT/LBM to be 5%

and 80% respectively , compared with 4% and 85% from simulation model. A good agreement between Kro from the study and SCAL data used for simulation model is indicated. However, Krw from the CT-calculated data and the SCAL results are in reasonable match only up to water saturation of 50%. A detailed comparison will be carried out when a wide range of samples from the same environment will be analyzed.

SUMMARY

This paper presents an example of core panoscopy, or multi-scale imaging, as part of a process for determining transport properties of a core sample. It presents the method and is part of a broader road map for determining rock properties through digital rock physics. Figure 9 summarizes the flow path of the paper. Digital x-ray micro-CT images of three resolutions were acquired. In the porosity calculations, low resolution images were used to partition the overall volume into its volume types, and high resolution images were used to populate the detailed porosity of the granular material into the low resolution images to yield an estimate of porosity. The granular portion of the sample was the dominant flow path determined through connectivity analysis. Therefore, the relative permeabilities for this portion of the sample were computed. The results from digital rock physics are in good agreement with measured values, although details cannot be released at this time due to confidentiality concerns. Core panoscopy is becoming an integral part of digital rock physics procedures. In heterogeneous rocks such as carbonates, proper digital rock physics may require even five or six registered resolutions to define mechanical and transport properties of core samples. This paper highlights the potential of digital rock physics and it was done in seven days with a shorter time possible in the near future.

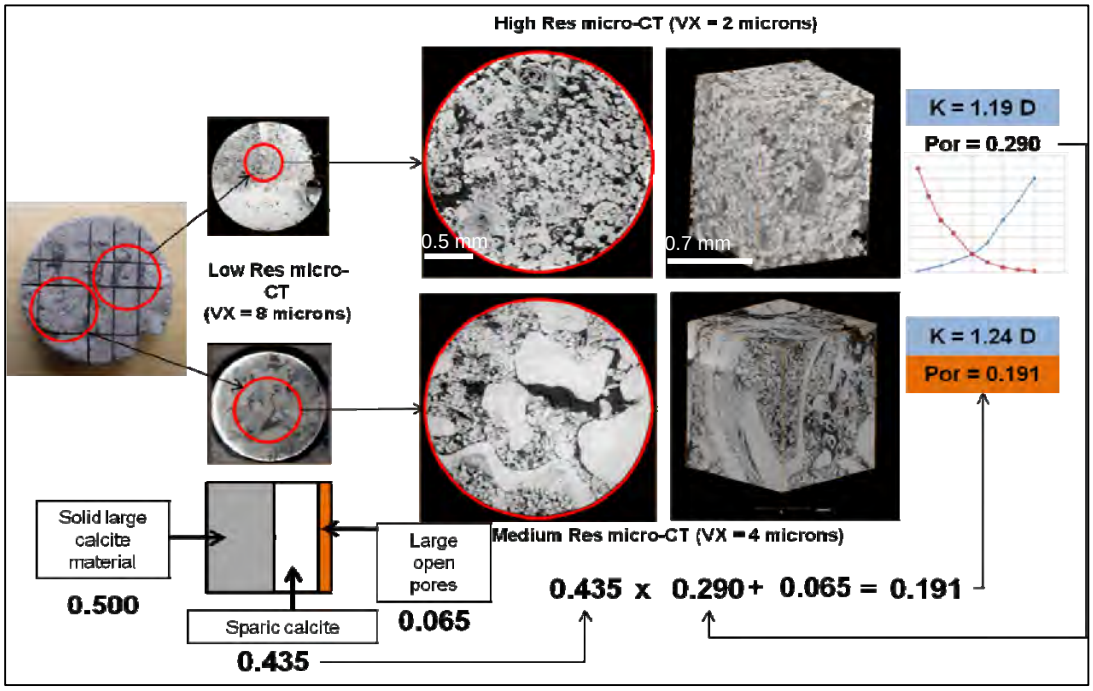

Figure 9: A summary of the multi-scale flow path described in this paper.

ACKNOWLEDGEMENTS

The authors express their sincere gratitude to ADNOC (Abu Dhabi National Oil Company), and its subsidiary operating company ADCO (Abu Dhabi Company for Onshore Oil Operations) in Abu Dhabi, United Arab Emirates, for kindly supplying the physical core sample material, previous analysis data, as well as for permitting our own analyses and the publication of these results.

REFERENCES

1. Alvarado, F. E., Grader, A. S. Halleck, P. M.: Visualization of Two- and Three-Phase Flow in Fractures Using X-ray Computed Tomography. Proceedings, SCA International Symposium, Trondheim, Norway, 12-16 September, 2006.
2. Arns, C. H., Knackstedt, M., Pinczewski, V., Garboczi, E. J.: Computation of Linear Elastic Properties from Microtomographic Images: Methodology and Agreement Between Theory and Experiment. *Geophysics*, Vol. 76, No. 3, September-October 2002, pp 1396-1405.
3. Bhatnagar, P., Gross, E., Krook, M.: A Model for Collisional Processes in Gasses I: Small Amplitude Processes in Charged and Neutral One-Component Syst*em*, Phys. Rev., **94**, pp 511, 1954.
4. Boltzmann, L.: Vorlesungen uber Gastheorie, (Barth Leizig 1896, 1898), engl. trans. S. G. Brush, *Lectures on Gas Theory*, Univ. Calif. Press, 1964.
5. Chapman, S., Cowling, T. G.: The Mathematical Theory of Non-Uniform Gases: an Account of the Kinetic Theory of Viscosity, Thermal Conduction, and Diffusion in Gases, Cambridge Univ. Press, 1970.
6. Cantrell, D. L. And Hagerty, R. M.: Microporosity in Arab Formation Carbonates, Saudi Arabia. *GeoArabia*, Vol. 4, No. 2, 1999, pp 129-154.
7. D'Humieres, D., Ginzburg, I., M. Krafczyk, M., Lallemand, P., Luo, L.: "Multiple-Relaxation-Time Lattice Boltzmann Models in Three Dimensions", Phil. Trans. R. Soc. Lond. A, **360**, pp 437, 2002.
8. Dvorkin, J., and Nur, A.: Scale of Experiment and Rock Physics Trends, *TLE*, Vol. 28, No. 1, January 2009, pp 110-115.
9. Dvorkin, J., Armbruster, M., Baldwin, C., Fang, Q., Derzhi, N., Gomez, C., Nur, B., Nur, A., and Mu, Y.: The Future of Rock Physics: Computational Methods versus Lab Testing, First Break, 26, September 2008, 63-68.
10. Gunstensen, A. and Rothman, D.: Lattice Boltzmann Model of Immiscible Fluids, Phys. Rev. A, **43**, pp 4320, 1991.
11. Knackstedt, M. A., Arns, C. H., Limaye, A., Sakellariou, A., Senden, T. J., Sheppard, A. P., Pinczewski, V., and Bunn, G. F.: Digital Core Laboratory: Properties of Reservoir Core Derived from 3D Images. Proceedings, SPE Asia Pacific Conference, 29-30 March, 2004.
12. Knackstedt, M., Latham, S., Madadi, M., Sheppard, A., Varslot, T., Arns, C.: Digital Rock Physics: 3D Imaging of Core Materials and Correlations to Acoustic and Flow Properties. *TLE*, Vol. 28, No. 1, January 2009, pp 28-33.
13. Principe, E. L.: High-density FIB-SEM 3D Nanotomography: with Applications of Real-Time Imaging During FIB Milling, Focused Ion Beam Systems: Basics and Applications, Nan Yao, Editor, Cambridge University Press (2007).
14. Principe, E. L.: Application of FIB in Combination with Auger Electron Microscopy". Focused Ion Beams: Instrumentation, Theory, Techniques and Practice, L. Gianuzzi, F. Stevie, eds., Springer (2002).
15. Shan, X. Chen, H.: Lattice Boltzmann Model for Simulating Flows with Multiple Phases and Components, Phys. Rev. E., **47**, pp 1815, 1993.
16. Swift, M., Osborne, W., Yeomans, J.: Lattice Boltzmann Simulations of Non-Ideal Fluids, Phys. Rev. Lett., **75**, pp 830, 1995.
17. Tkachuk, A., Duewer, F., Cui, H., Feser, M., Wang, S., Yun, W.: X-ray Tomography in Zernike Phase Contrast Mode @ 8 keV with 50 nm Resolution, Using Cu Rotating X-ray Source. Z. Kristallogr. 222 (2007) pp 650-655.

18. Touati, M., Funk, J., Cinar, Y., Knackstedt, M.: Pore Network Modeling of Saudi Aramco Rocks: A Comparative Study. Proceedings, SPE Saudi Arabia Section Technical Symposium, 09-11 May, 2009.
19. YoungSeuk, K., Mukerji, T., and Nur, A.: Computational Rock Physics at the Pore Scale: Transport Properties and Diagenesis in Realistic Pore Geometries TLE, Vol. 20, pp 180-183.